Electronic Supplementary Material (ESI) for Journal of Materials Chemistry A.

# *Supporting Information*

# Tailoring Trimetallic CoNiFe Oxide Nanostructured Catalysts for the Efficient Electrochemical Conversion of Methane to Methanol

Libin Zeng, Antony R. Thiruppathi, Joshua van der Zalm, Tony Shi, Aicheng Chen*

Electrochemical Technology Center, Department of Chemistry, University of Guelph, 50 Stone Road East, Guelph, ON N1G 2W1, Canada

*Corresponding author. E-mail: aicheng@uoguelph.ca

## Experimental Section

### 1. Chemicals

Nickel (II) nitrate hexahydrate (99%, $Ni(NO_3)_2 \cdot 6H_2O$), cobalt (II) nitrate hexahydrate (98%, $Co(NO_3)_2 \cdot 6H_2O$), sodium citrate (99%, $Na_3C_6H_5O_7$), potassium hexacyanoferrate (III) ($99\%^+$, $K_4Fe(CN)_6$), sodium sulfate (99%, $Na_2SO_4$), sodium carbonate ($99\%^+$, $Na_2CO_3$), sodium hydroxide ($97\%^+$, NaOH), sodium salicylate (99%, $C_7H_5O_3Na$), sodium hypochlorite (5%, NaClO), sodium nitroferricyanide (III) ($99\%^+$, $C_5FeN_6Na_2O$), hydrazine ($98\%^+$, $N_2H_4$), and ammonium chloride ($99\%^+$, $NH_4Cl$) were purchased from Sigma-Aldrich Chemical Reagent Ltd.. Nafion (1 wt.%) solution, hydrogen peroxide (30%, $H_2O_2$), sulfuric acid ($99\%^+$), methanol and ethanol were purchased from Aladdin Ltd. All reagents were of analytical grade and used without further purification. Additionally, an anion exchange membrane (AEM) was purchased from the DuPont Company (N2050TX, thickness: 0.3 mm). The deionized (DI) water (18.2 MΩ cm) used in all experiments was obtained from a Nanopure Diamond™ ultrapure water system.

## 2. Electrochemical activity evaluation

A two-chamber cell separated by a pre-treated cation exchange membrane (CEM) was used to investigate the products of each chamber. When a single reduction or oxidation reaction was investigated in one chamber, the other chamber was examined without gas bubbling. The iR drop was uncompensated during the electrochemical measurements. For the NRR experiments, a graphite rod was used as the counter electrode. In the cathode chamber with $N_2$ gas, the generation of ammonia ($NH_3$) was measured and quantitatively analyzed by the modified indophenol blue method.[1, 2] As follows, 2 mL of the cathode effluent was taken, then 2 mL of solution A (10.0 g salicylic acid and 10.0 g sodium citrate dissolved in 0.32 M NaOH solution), 1 mL 0.05 M NaClO and 0.2 mL of 0.01 g mL$^{-1}$ $C_5FeN_6Na_2O$ was dropped into the testing solution in turn. After 2-hours, the concentration was measured at 655 nm by UV-vis spectrophotometer (Varian Cary 50). A calibration curve was generated using0.0, 0.2, 0.4, 0.6, 0.8 and 1.0 µg mL$^{-1}$ of standard $NH_4Cl$ vs. the corresponding UV-vis absorbance, giving a clear linear relationship ($y = 0.113 x + 0.013$, $R^2 = 0.999$) in triplicate parallel experiments. The control experiments under the $N_2$-saturated, Ar-saturated and open-circuit conditions for the NRR have been performed to avoid any exogenous sources of nitrogen compounds.[3] The generated $C_{[NH_3]}$ in the NRR was calculated as follow:

$$C_{[NH_3]} = C_{[NH_3]}^{N_2} - C_{[NH_3]}^{Ar} - C_{[NH_3]}^{Open} \qquad \text{(S1)}$$

where $C_{[NH_3]}^{N_2}$, $C_{[NH_3]}^{Ar}$, $C_{[NH_3]}^{Open}$ are obtained under the $N_2$-saturated, Ar-saturated and open-circuit conditions for the NRR experiments, respectively.

The $NH_3$ yield was calculated by the following equation:

$$NH_3 \text{ yield} = C_{[NH_3]} * V/(m_{cat.} * t) \tag{S2}$$

where $C_{[NH_3]}$ is the obtained $NH_3$ concentration; V is the reaction electrolyte solution (20 mL); $m_{cat.}$ is the mass of the catalyst, and t is the time of electrolysis reaction (t = 2 h).

Faradaic efficiency was obtained as follows:

$$FE = 3*F*C_{[NH_3]} * V/(18 * Q) \tag{S3}$$

where F is the Faraday constant (96485.3 C $mol^{-1}$); Q is the quantity of electric charge by the applied potential. Besides, the potential by-product ($N_2H_4$) was also investigated by our formerly reported method.[4] There was no change for the initial and 2 h for the NRR in the UV-vis spectrum at 455 nm, suggesting that there is no any $N_2H_4$ generation in this system.

In the anode chamber, the $CH_4$ oxidation reaction was investigated. The pure $CH_4$ gas was continuously purged into 0.5 M $Na_2CO_3$ electrolyte at a flow rate of 5 mL $min^{-1}$. All the gas products were detected by gas chromatography. Liquid products of the $CH_4$ electrochemical oxidation were analyzed by $^1H$ nuclear magnetic resonance spectroscopy ($^1H$ NMR) measured on a 600 MHz NMR spectrometer (Bruker). Before the measurement, a 0.35 mL sample from the anode chamber was mixed with 0.05 wt% tetramethylsilane (TMS) in 0.35 mL $D_2O$. The yield of products, FEs, the corresponding selectivity, and the $CH_4$ conversion rate were calculated as follows:

$$\text{Yields (mmol } g_{cat.}^{-1} h^{-1}) = \text{mmol of products / g of catalysts / h of the reaction time} \tag{S4}$$

$$FE\ (CH_3OH, \%) = 0.1929 * n\ (CH_3OH, \mu mol) * 100\% / Q \tag{S5}$$

$$FE\ (CH_3CHOHCH_3, \%) = 0.1929 * n\ (CH_3CHOHCH_3, \mu mol) * 100\% / Q \tag{S6}$$

Selectivity of $CH_3OH$ = 100% * n ($CH_3OH$) / ( n ($CH_3OH$) + n ($CH_3CHOHCH_3$) (S7)

Selectivity of $CH_3CHOHCH_3$ = 100% * n ($CH_3CHOHCH_3$) / (n ($CH_3OH$) + n ($CH_3CHOHCH_3$) (S8)

where Q is the total quantity of the electric charge.

The integrated reaction system was comprised of two working electrodes and one reference electrode. Where the optimized $Co_{0.8}Ni_{0.2}Fe_2O_4$-N/C and $Co_{0.6}Ni_{0.4}Fe_2O_4$-N/C catalysts were employed as the working electrodes in the cathode and anode chambers, respectively. $N_2$ gas and $CH_4$ gas were simultaneously purged into the corresponding electrolytes. Considering the measurement of the current density, the reference electrode would be employed in the same chamber with the targeted reaction. After two-hour electrolysis, the corresponding anode- and cathode-electrolyte would be collected and further analyzed. Blank experiments, including NiCoFe catalysts under the open potential condition, were carried out to eliminate possible interferences.

## 3. Characterization of nanomaterials

The morphologies of CoNiFe-N/C and CoNiFe catalysts were characterized using a field-emission scanning electron microscope (FE-SEM) (FEI Quanta 250) and the high-resolution transmission electron microscopy (HRTEM) (FEI Tecnai F30 electron microscope, using a 200 kV accelerating voltage). An X-ray diffractometer with Cu $K\alpha$ radiation (D/max-2400, Japan, source light at the wavelength ($\lambda$) of 0.1541 nm) was employed to investigate the crystallinity structure of the as-prepared catalysts. X-ray Photoelectron Spectroscopy (XPS) (Scienta Omicron) with a monochromatic Al $K_\alpha$ x-ray source was used to analyze their chemical composition and oxidation states. Raman spectra were recorded at 532 nm by utilizing a Raman spectrophotometer (Renishaw

Canada Ltd.). Thermogravimetric (TG) analysis was performed with a QMA200M thermal analyzer (METTLER TOLEDO) at a heating rate of 2 °C min$^{-1}$ under air conditions. The radicals were detected via electron paramagnetic resonance (EPR) spectroscopy, which was conducted with a Bruker ECS106 X-band spectrometer (Bruker A200, Germany). The gas products were transferred using a gas-tight syringe (Hamilton) and examined using a gas chromatograph (GC, Shimadzu, GC-2014, Column:silica gel) that was equipped with a thermal conductive detector (TCD).

## 4. Theoretical calculations

To explore the electronic structures and electron transfer in the NRR and $CH_4$ oxidation systems, the $Co_yNi_{1-y}Fe_2O_4$ and $Co_yNi_{1-y}Fe_2O_4$-N/C with one layer of carbon structure models were built based on the $NiFe_2O_4$ template. The optimization of the constructed structures was enabled by the CASTEP module with the Perdew-Burke-Ernzerhof (PBE) functional of the generalized gradient approximation (GGA). Additionally, the position of the Co doping was thought to be the replacement of Ni atoms with Co atoms. A 2 × 2 × 1 3D triclinic $NiFe_2O_4$ cell ($a = 8.480$ Å, $b = 8.480$ Å, $c = 8.480$ Å, $\alpha = \beta = \gamma = 90°$) was used for the doping and the addition of carbon layer cells. A k-point set of 2 × 1 × 1 and an energy cut-off of 320 eV were performed to optimize the geometry of the constructed models with medium k-point set. The convergence criterion was $1.0 \times 10^{-5}$ eV for energy and 0.05 eV Å$^{-1}$ for force. The adsorption energy (E) was calculated as follow:

$$\triangle E_{Co_yNi_{1-y}}(CH3) = E^{Total}_{Co_yNi_{1-y}-Carbon\ layer}(CH3) - E^{Total}_{Co_yNi_{1-y}}(CH3) - E_{Carbon\ layer} - E_{CH_4} + E_H$$

(S9)

where $E_{Co_yNi_{1-y}-Carbon\ layer}^{Total}(CH3)$, $E_{Co_yNi_{1-y}}^{Total}(CH_3)$, $E_{Carbon\ layer}$, $E_{CH_4}$ and $E_H$ are the electronic energies of the $Co_yNi_{1-y}Fe_2O_4$-N/C, $Co_yNi_{1-y}Fe_2O_4$, carbon, $CH_4$ and H unit cell, respectively. For the first principle calculation of the activation of $CH_4$ to·$CH_3$, an energy cut-off of 350 eV was performed. A force tolerance, SCF tolerance, and electronic field were 0.05 eV $Å^{-1}$, $1.0 \times 10^{-5}$ eV per atom and -5 eV vs. Vacuum, respectively. The experimental optimal potential on the electrode reaction was performed by adding the value of -n eU (n: the number of electrons in the DMC; U: the electric potential).

**Table S1**. Yields of $Co_yNi_{1-y}$-Fe PBA catalysts after the high-temperature treatment under the Air-

| Co-doping rate | Air condition treatment (350℃)[a] | Yield[a] | Ar condition treatment (350℃)[b] | Yield[b] |
|---|---|---|---|---|
| 0 | $NiFe_2O_4$ | 55.4% | $NiFe_2O_4$/N@C | 56.2% |
| 20% | $Co_{0.2}Ni_{0.8}Fe_2O_4$ | 60.9% | $Co_{0.2}Ni_{0.8}Fe_2O_4$/N@C | 72.1% |
| 40% | $Co_{0.4}Ni_{0.6}Fe_2O_4$ | 67.1% | $Co_{0.4}Ni_{0.6}Fe_2O_4$/N@C | 77.1% |
| 60% | $Co_{0.6}Ni_{0.4}Fe_2O_4$ | 65.0% | $Co_{0.6}Ni_{0.4}Fe_2O_4$/N@C | 67.3% |
| 80% | $Co_{0.8}Ni_{0.2}Fe_2O_4$ | 61.1% | $Co_{0.8}Ni_{0.2}Fe_2O_4$/N@C | 63.6% |
| 100% | $CoFe_2O_4$ | 53.9% | $CoFe_2O_4$/N@C | 62.1% |

or Ar-condition.

| Sample | C/At% | N/At% | O/At% | Fe/At% | Ni/At% | Co/At% |
|---|---|---|---|---|---|---|
| CoNiFe-N/C-0 | 51.28 | 37.03 | 10.08 | 0.49 | 1.31 | 0 |
| CoNiFe-N/C-0.2 | 50.89 | 38.41 | 8.89 | 0.62 | 0.98 | 0.21 |
| CoNiFe-N/C-0.4 | 50.77 | 38.57 | 8.33 | 0.68 | 1.06 | 0.59 |
| CoNiFe-N/C-0.6 | 50.54 | 38.31 | 8.36 | 0.87 | 0.73 | 1.19 |
| CoNiFe-N/C-0.8 | 50.31 | 38.07 | 8.60 | 1.06 | 0.34 | 1.62 |
| CoNiFe-N/C-1 | 50.17 | 37.94 | 8.73 | 1.28 | 0 | 1.88 |

**Table S2**. EDX analysis of different $Co_yNi_{1-y}Fe_2O_4$-N/C catalysts

**Table S3**. Parameter analysis of the equivalent circuit model corresponding to the Nyquist plots of the as-prepared $Co_yNi_{1-y}Fe_2O_4$-C/N under $N_2$-saturated conditions.

| **$N_2$-saturated** | **$R_{ohm}$ (Ω)** | **$C_{CE}$ (μF)** | **$R_{ct(CE)}$ (Ω)** | **$C_{AE}$ (μF)** | **$R_{ct(AE)}$ (kΩ)** | **W(S*Sec$^5$)** |
|---|---|---|---|---|---|---|
| 0 | 90.4 ± 0.06 | 2.38 ± 0.05 | 4187 ± 0.06 | 8.04 ± 0.01 | 0.18 ± 0.03 | 0.027 ± 0 |
| 0.2 | 92.6 ± 0.04 | 7.17 ± 0.04 | 1850.9 ± 0.04 | 2.87 ± 0.06 | 1.64 ± 0.05 | 0.026 ± 0 |
| 0.4 | 89.8 ± 0.01 | 4.19 ± 0.04 | 2071.7 ± 0.07 | 2.64 ± 0.02 | 1.21 ± 0.01 | 0.0003 ± 0 |
| 0.6 | 88.4 ± 0.07 | 1.53 ± 0.02 | 1276 ± 0.08 | 8.98 ± 0.01 | 0.074 ± 0 | 0.0004 ± 0 |
| 0.8 | 86.3 ± 0.01 | 2.65 ± 0.03 | 541.8 ± 0.02 | 17.5 ± 0.03 | 0.013 ± 0 | 0.0004 ± 0 |
| 1 | 91.5 ± 0.07 | 16.1 ± 0.09 | 6861 ± 5 | 1.76 ± 0.01 | 1.18 ± 0.002 | 0.0003 ± 0 |

$R_{ohm}$ = Resistance of solution, $R_{ct(CE)}$ = Charge transfer resistance, $R_{ct(AE)}$ = Charge transfer and recombination resistance, C = Capacitance of double layer, W = Warburg impedance (mass transfer).

**Table S4.** Parameter analysis of the equivalent circuit model corresponding to the Nyquist plots of the as-prepared $Co_yNi_{1-y}Fe_2O_4$-C/N under the $CH_4$-saturated conditions.

| **$CH_4$-saturated** | **$R_{ohm}$ (Ω)** | **$C_{CE}$ (μF)** | **$R_{ct(CE)}$ (Ω)** | **$C_{AE}$ (mF)** | **$R_{ct(AE)}$ (kΩ)** | **W(S*Sec$^5$)** |
|---|---|---|---|---|---|---|
| 0 | 37.8 ± 0.02 | 1.72 ± 0.02 | 1352 ± 0.04 | 0.02 ± 0 | 2.04 ± 0.04 | 0.0003 ± 0 |
| 0.2 | 34.7 ± 0.03 | 7.08 ± 0.05 | 404.1 ± 0.05 | 3.34 ± 0.03 | 1.96 ± 0.05 | 0.0003 ± 0 |
| 0.4 | 32.1 ± 0.02 | 2.11 ± 0.01 | 40.3 ± 0.03 | 0.002 ± 0 | 1.17 ± 0 | 0.0007 ± 0 |
| 0.6 | 24.0 ± 0.01 | 1.23 ± 0.02 | 38.8 ± 0.03 | 2.34 ± 0.03 | 0.52 ± 0.01 | 0.0024 ± 0 |
| 0.8 | 26.5 ± 0.02 | 1.19 ± 0.03 | 81.8 ± 0.06 | 0.004 ± 0 | 2.39 ± 0.03 | 0.001 ± 0 |
| 1 | 25.2 ± 0.01 | 1.33 ± 0.02 | 264.7 ± 0.04 | 0.008 ± 0 | 2.55 ± 0.01 | 0.0007 ± 0 |

$R_{ohm}$ = Resistance of solution, $R_{ct(CE)}$ = Charge transfer resistance, $R_{ct(AE)}$ = Charge transfer and recombination resistance, C = Capacitance of double layer, W = Warburg impedance (mass transfer).

**Table S5.** Comparison of electrochemical ammonia synthesis by $N_2$ fixation at the Co/Ni/Fe-based catalysts.

| **Catalysts** | **Conditions** | **Faradaic Efficiency (%)/ Bias (V *vs.* RHE)** | **Ammonia Yield ($\mu$g $h^{-1}$ $mg^{-1}_{cat.}$)/Bias (V *vs.* RHE)** | **Ref.** |
|---|---|---|---|---|
| $CoMoO_4$ nanoparticles | 0.1 M $Na_2SO_4$ | 10.18/-0.3 | 23.14/-0.3 | 5 |
| CoO QDs/rGO | 0.1 M $Na_2SO_4$ | 8.30/-0.6 | 21.50/-0.7 | 6 |
| $CoFe_2O_4$/rGO | 0.1 M $Na_2SO_4$ | 6.20/-0.4 | 5.14/-0.4 | 7 |
| Co-N/C | 0.1 M KOH | 10.10/-0.1 | 5.10/-0.4 | 8 |
| $C_3O_4$/NC nanocages | 0.05 M $H_2SO_4$ | 8.50/-0.2 | 42.58/-0.2 | 9 |
| Co SAs-N/C | 0.05 M $H_2SO_4$ | 10.50/-0.2 | 2.09/-0.2 | 10 |
| Ni/NiO/C nanotubes | 0.1 M KOH | 10.9/-0.7 | 43.15/-0.7 | 11 |
| N-NiO/CC nanosheets | 0.1 M $LiClO_4$ | 7.30/-0.5 | 22.70/-0.4 | 12 |
| NiO QDs/graphene | 0.1 M $Na_2SO_4$ | 7.80/-0.7 | 18.60/-0.7 | 13 |
| $NiCo_2O_4$-N/C | 0.1 M $Na_2SO_4$ | 5.30/-0.25 | 17.80/-0.25 | 14 |
| $Fe_2O_3$ nanorods | 0.1 M $Na_2SO_4$ | 0.94/-0.8 | 15.90/-0.8 | 15 |
| $Fe_2O_3$/rGO | 0.1 M $LiClO_4$ | 5.89/-0.5 | 22.13/-0.5 | 16 |
| Fe/$Fe_3O_2$/C | 0.2 M $NaHCO_3$ | 6.25/-0.3 | 15.91*/-0.3 | 17 |
| Fe SAs/N-O/C | 0.1 M HCl | 11.80/-0.4 | 31.90/-0.4 | 18 |
| FeMo-N/C | 0.1 M $H_2SO_4$ | 14.2/-0.1 | 38.76/-0.1 | 19 |
| Fe-N/C-carbon nanotube | 0.1 M KOH | 9.28/-0.2 | 34.83/-0.2 | 20 |
| FeNi-N/C | 0.1 M $Na_2SO_4$ | 1.75/-0.2 | 23.34/-0.3 | 4 |
| $Co_{0.8}Ni_{0.2}Fe_2O_4$-N/C | 0.1 M $Na_2SO_4$ | 15.35/-0.7 | 52.56/-0.8 | This work |

*Its unit is $\mu$g $h^{-1}$ $cm^{-2}_{cat}$;

**Table S6**. Comparison of $CH_4$ oxidation performance at 0.8 V vs Ag/AgCl for 2 h with or without $N_2$ gas flow in the cathode chamber.

| **NRR** | **Methanol yield**$^1$ | **Its FE** | **2-propanol yield**$^1$ | **Its FE** | **Current density**$^2$ |
|---|---|---|---|---|---|
| Yes | 1925.4 | 9.03% | 398.1 | 5.59% | 4.1 |
| No | 722.6 | 3.76% | 306.4 | 4.79% | 2.9 |

$^1$Unit: mmol $g_{cat}^{-1}$ $h^{-1}$, $^2$Unit: mA $cm^{-2}$.

**Table S7**. Comparison of the NRR performance at -0.8 V vs Ag/AgCl for 2 h with or without $CH_4$ gas in the anode.

| **DMC** | **Ammonia yield ($\mu$g h$^{-1}$ mg$^{-1}_{cat.}$)** | **Its FE** | **Hydrazine yield ($\mu$g h$^{-1}$ mg$^{-1}_{cat.}$)** | **Its FE** | **Current density (mA cm$^{-2}$)** |
|---|---|---|---|---|---|
| Yes | 10.69 | 5.18% | 0 | 0 | 1.23 |
| No | 6.73 | 4.67% | 0 | 0 | 0.84 |

**Table S8**. Summaries of electrocatalytic $CH_4$ oxidation systems at room temperature.

| Catalyst | Potential | Main Product | Product Yield ($^{a}$mmol g$^{-1}$ h$^{-1}$/$^{b}$mg mL$^{-1}$ h$^{-1}$) | Reference |
|---|---|---|---|---|
| $TiO_2$-ALD | 0.6 V vs. RHE | CO | --- | 21 |
| NiO/Ni | 1.4 V vs. RHE | $CH_3CH_2OH$ | $^{a}$0.025 | 22 |
| NiO/Ni hollow fiber | 1.46 V vs. RHE | $CH_3CH_2OH$ | --- | 23 |
| $NiO/ZrO_2$ | 2.0 V vs. SCE | CO | --- | 24 |
| $ZrO_2/NiCo_2O_4$ | 2.0 V vs. Pt | $CH_3CH_2CH_2OH$,<br>$CH_3CH(OH)CH_3$ | $^{a}$2.595 | 25 |
| $ZrO_2/Co_3O_4$ | 2.0 V vs. Pt | $CH_3CH_2CH_2OH$,<br>$CH_3CH(OH)CH_3$ | $^{b}$0.22 | 26 |
| $ZrO_2$ NTs/$Co_3O_4$ | 1.6 V vs. RHE | $CH_3CH_2CH_2OH$,<br>$CH_3CH(OH)CH_3$<br>$CH_3CH_2OH$ | $^{a}$9.36 | 27 |
| $ZrO_2/CuO_x$ | 2.2 V vs. RHE | $CH_3CH_2CH_2OH$,<br>$CH_3CH(OH)CH_3$ | $^{b}$0.23 | 28 |
| $CuO/CeO_2$ | 1.5 V vs. Pt | $CH_3OH$ | $^{a}$0.753 | 29 |
| $Co_{0.6}Ni_{0.4}Fe_2O_4$-N/C | 0.8 V vs. Ag/AgCl | $CH_3OH$<br>$CH_3CH(OH)CH_3$ | $^{a}$1029/$^{b}$0.08 | This work |
| $Co_{0.6}Ni_{0.4}Fe_2O_4$-N/C* | 1.1 V vs. Ag/AgCl | $CH_3OH$<br>$CH_3CH(OH)CH_3$ | $^{a}$7273.8/$^{b}$0.74 | This work |
| $Co_{0.6}Ni_{0.4}Fe_2O_4$-N/C* | 0.8 V vs. Ag/AgCl | $CH_3OH$<br>$CH_3CH(OH)CH_3$ | $^{a}$2323.5/$^{b}$0.24 | This work |

* The integrated electrochemical system.

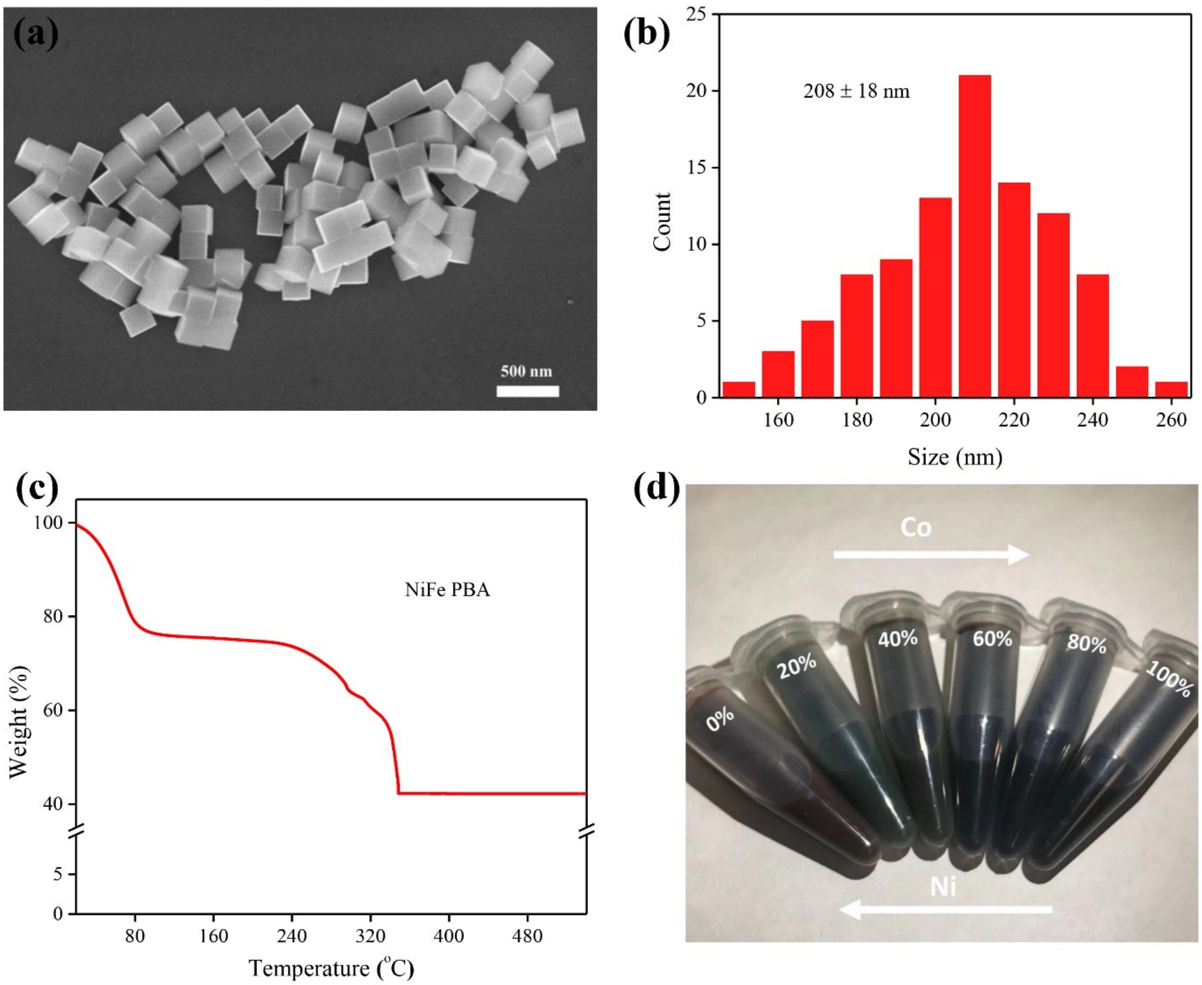

**Figure S1**. (a) SEM image and (b) corresponding size distributions of NiFe PBA template catalyst; (c) Thermogravimetry curve of the NiFe PBA template under air conditions at heating rate of 2 °C min$^{-1}$; (d) Image of the different ratios of CoNiFe-N/C catalyst inks.

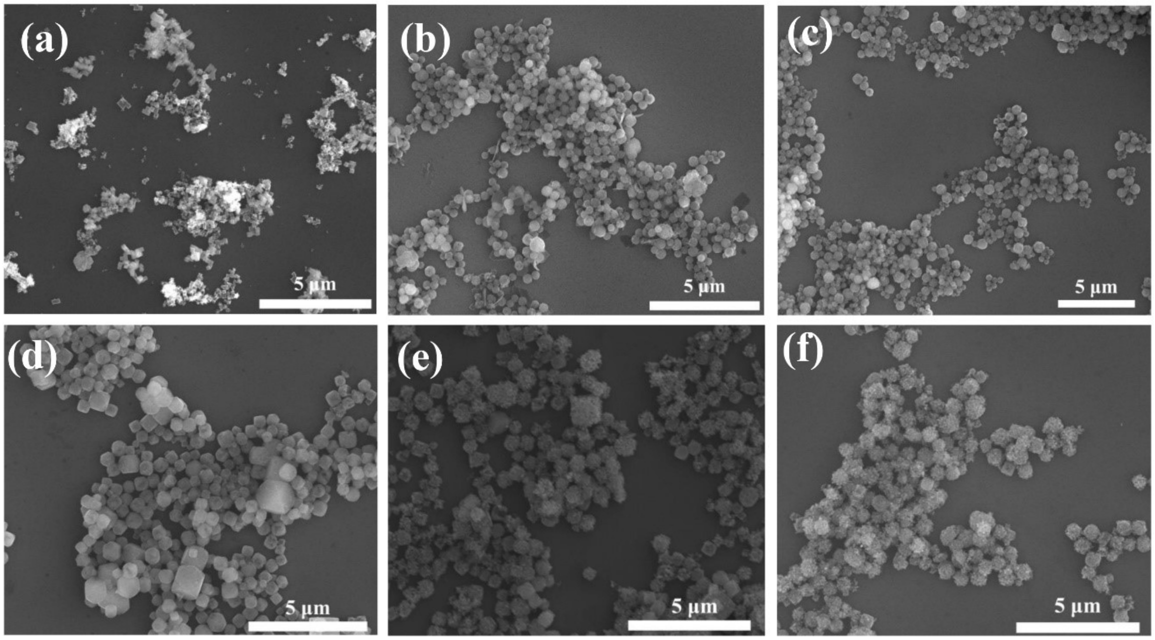

**Figure S2**. SEM images of $Co_yNi_{1-y}$-$Fe_2O_4$-N/C catalysts, (a) y=0, (b) y=0.2, (c) y=0.4, (d) y=0.6, (e) y=0.8, and (f) y=1, respectively.

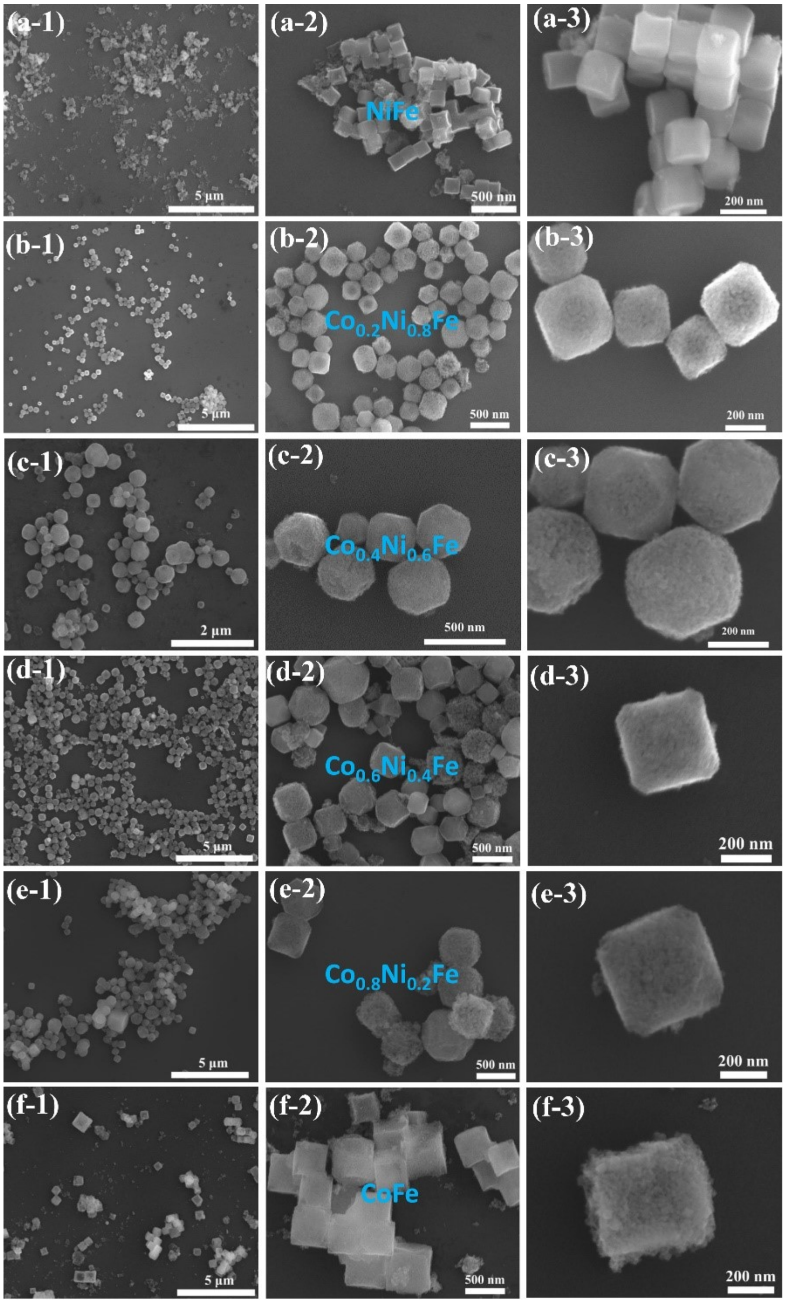

**Figure S3**. SEM images of $Co_yNi_{1-y}$-$Fe_2O_4$ catalysts, (a) y=0, (b) y=0.2, (c) y=0.4, (d) y=0.6, (e) y=0.8, and (f) y=1, respectively.

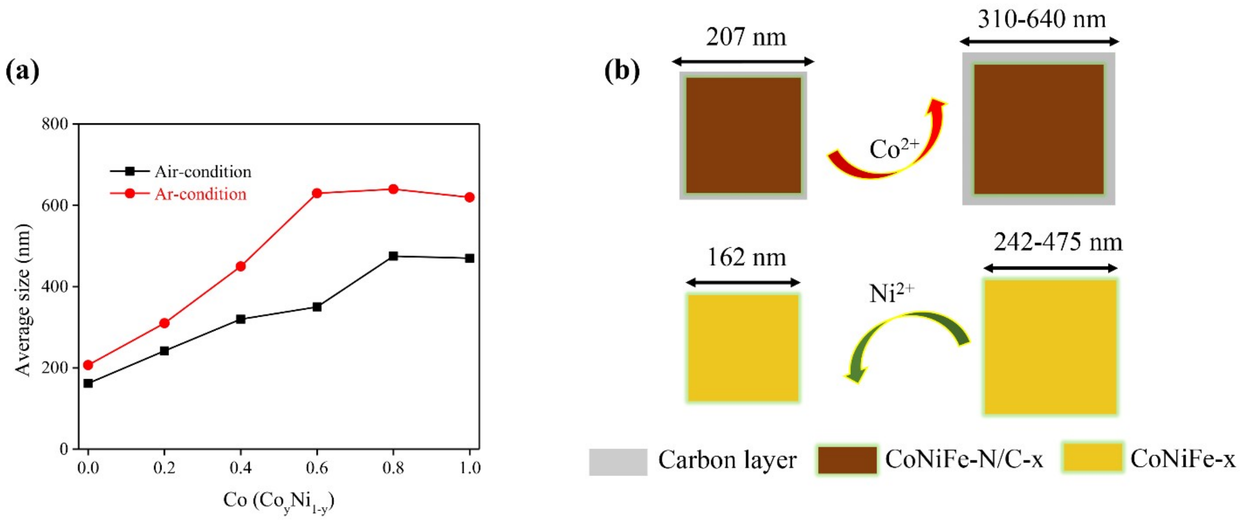

**Figure S4**. (a) Average size of $Co_yNi_{1-y}$-$Fe_2$ PBA derived catalysts under Air- and Ar-conditions, respectively; (b) Scheme of the structure proposed for the PBA particles in CoFeNi. The scale between the core and the shell is arbitrary.

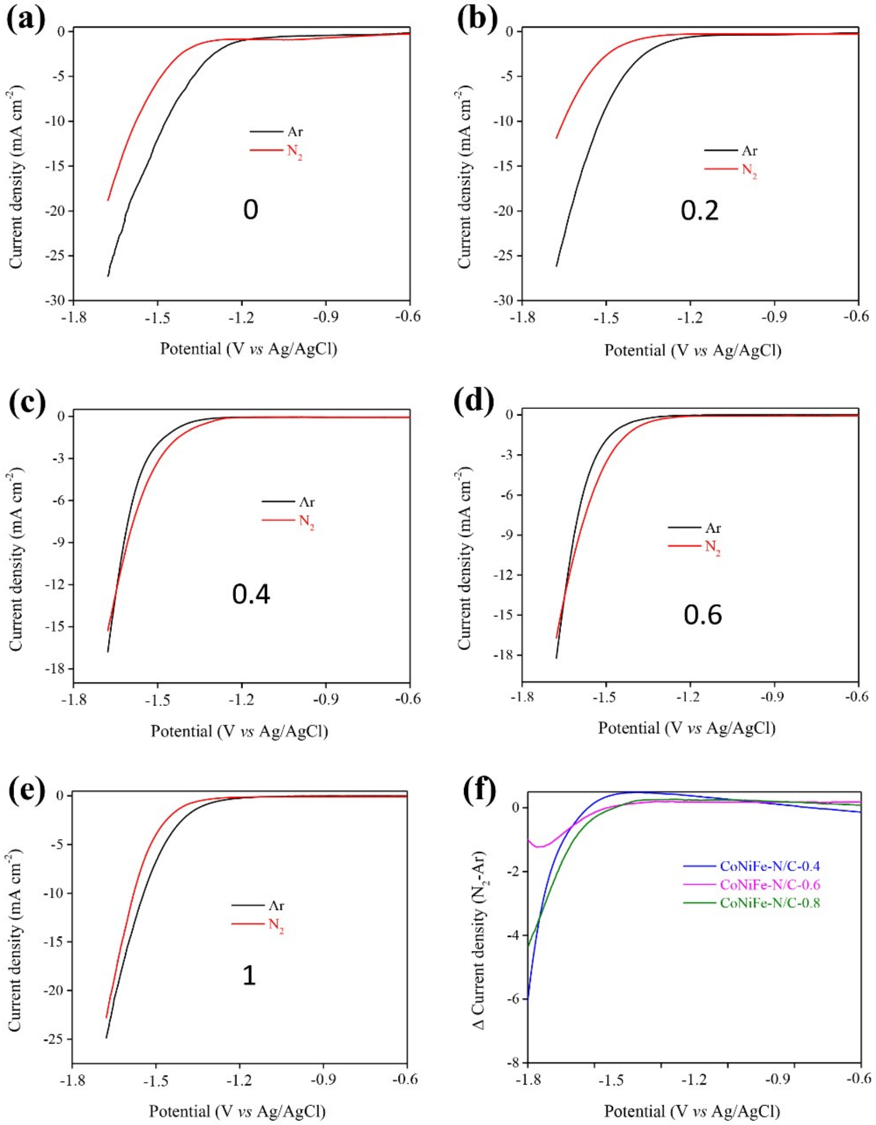

**Figure S5**. (a)-(e) LSV curves of CoNiFe-N/C-x (x= 0, 0.2, 0.4, 0.6, 1) catalysts in Ar- and N$_2$-saturated 0.1 M Na$_2$SO$_4$ solution with a scan rate of 20 mV s$^{-1}$, respectively. (f) the corresponding current density difference of the CoNiFe-N/C catalysts measured at the N$_2$-saturated and the Ar-saturated solution.

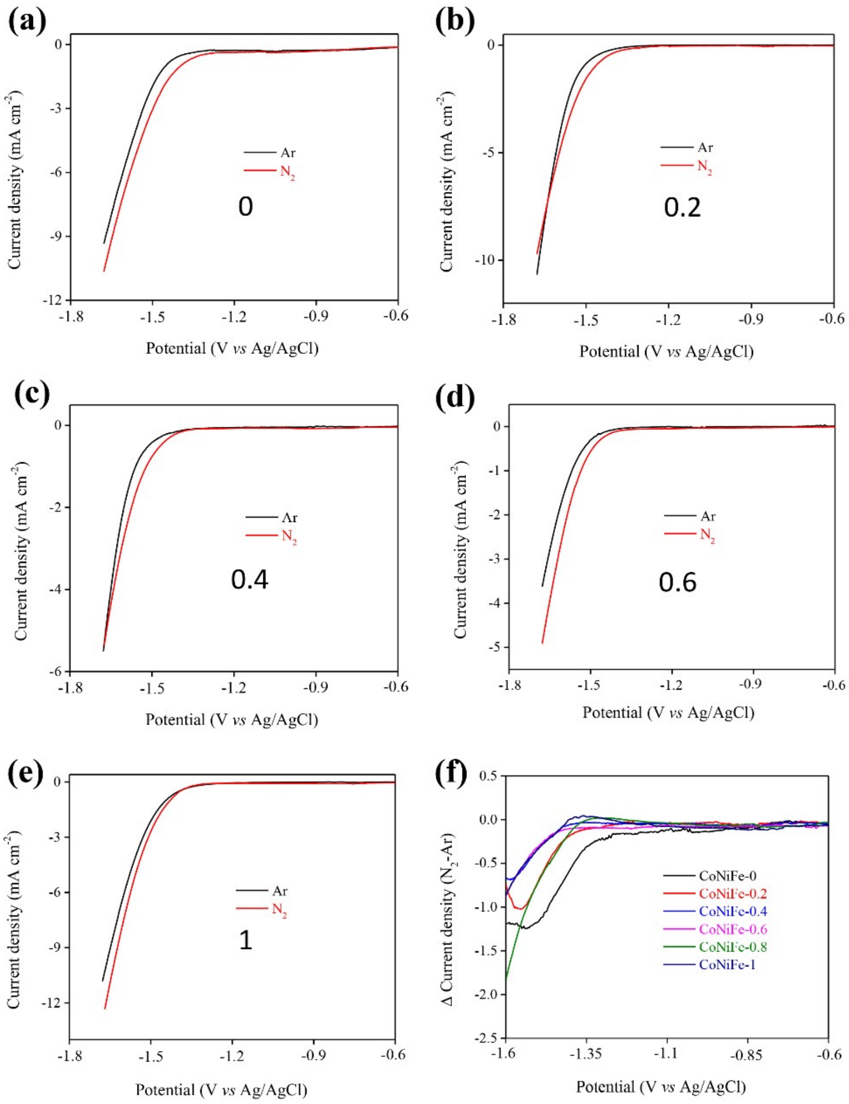

**Figure S6**. (a)-(e) LSV curves of CoNiFe-x (x= 0, 0.2, 0.4, 0.6, 1) catalysts in Ar- and N$_2$-saturated 0.1 M Na$_2$SO$_4$ solution with a scan rate of 20 mV s$^{-1}$, respectively. (f) the corresponding current density difference of the CoNiFe-x catalysts measured at the N$_2$-saturated and the Ar-saturated solution.

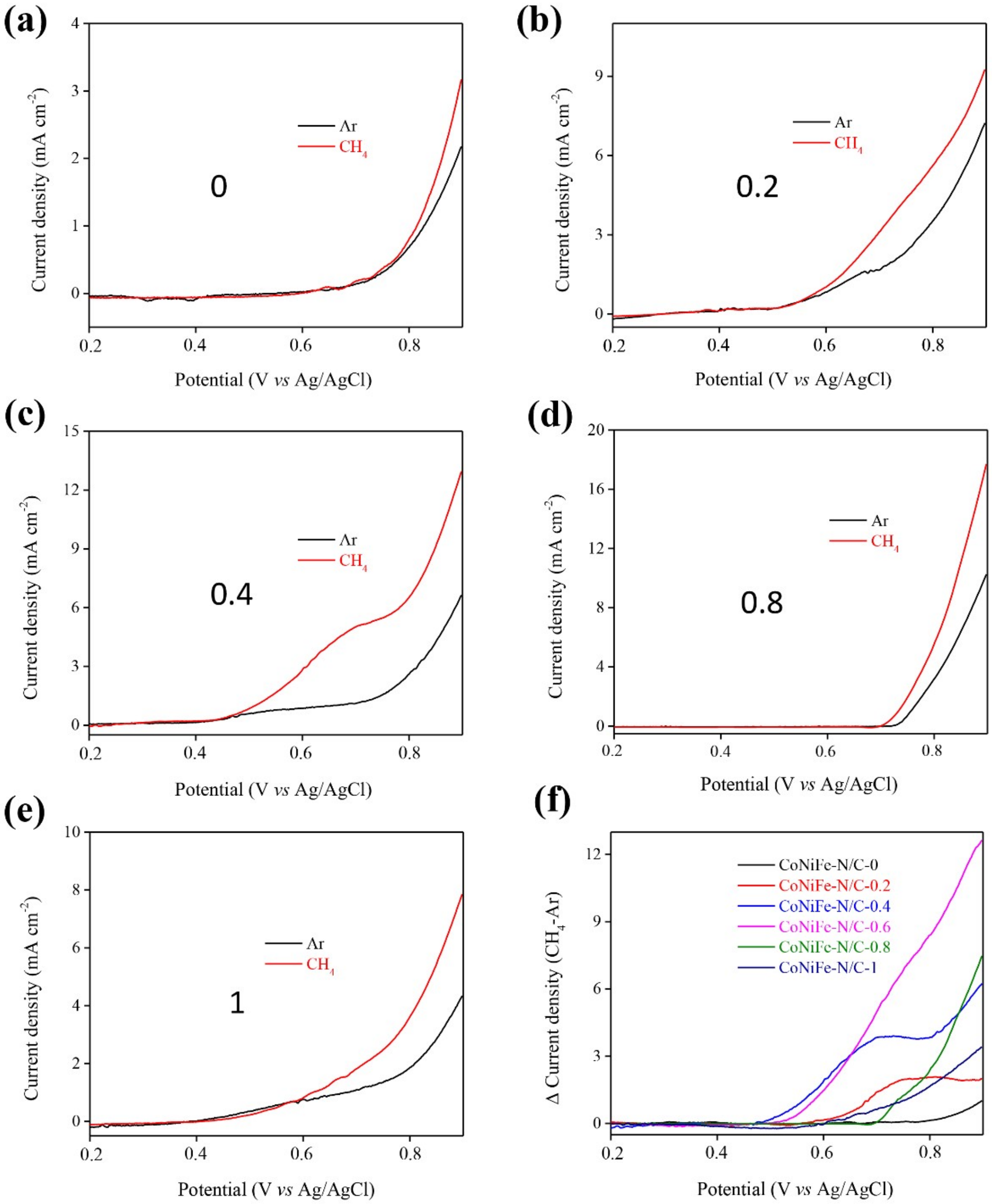

**Figure S7**. (a)-(e) LSV curves of CoNiFe-N/C-x (x= 0, 0.2, 0.4, 0.8, 1) catalysts in Ar- and $CH_4$-saturated 0.5 M $Na_2CO_3$ solution with a scan rate of 20 mV $s^{-1}$, respectively. (f) current density difference of the CoNiFe-N/C-x catalysts measured at the $CH_4$-saturated and the Ar-saturated solution.

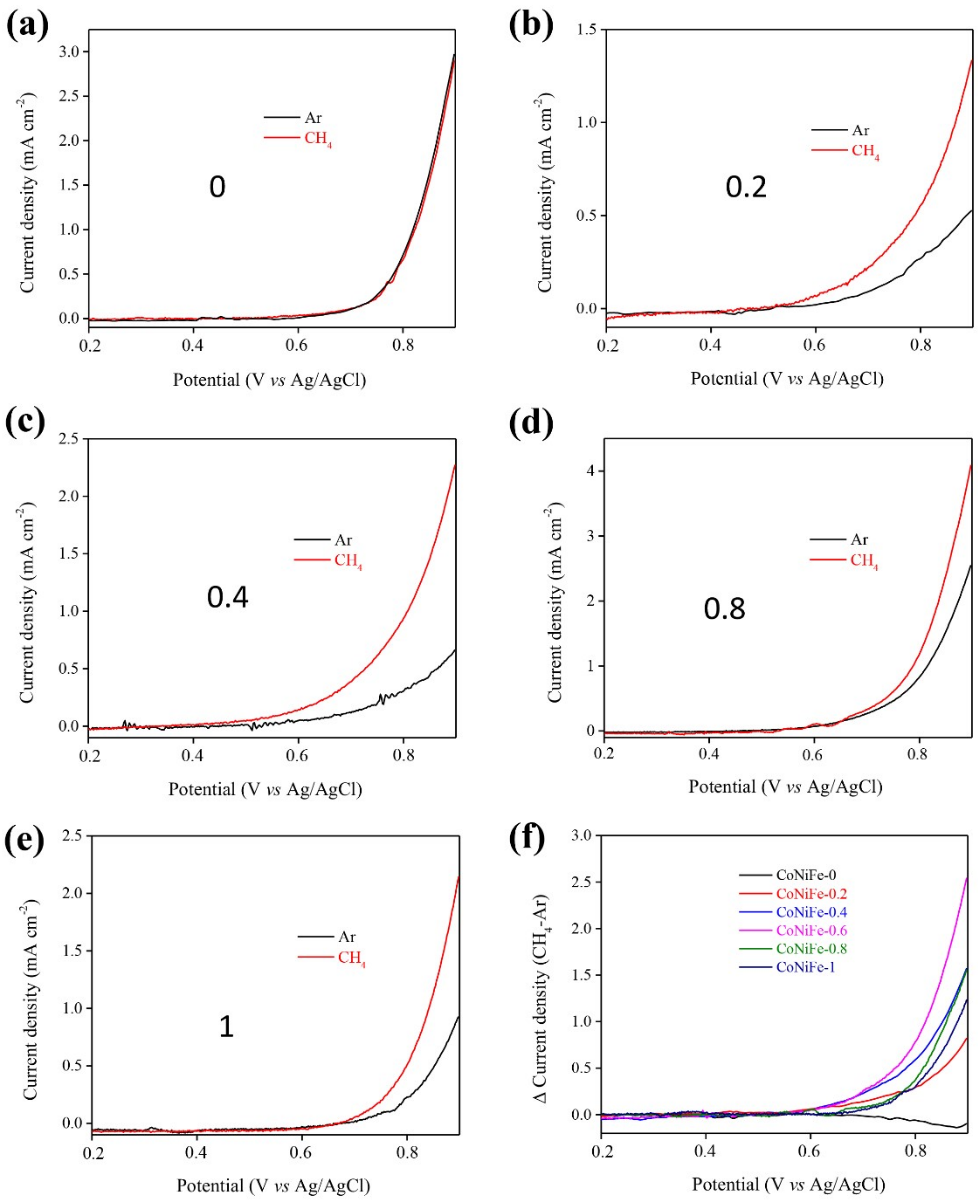

**Figure S8**. (a)-(e) LSV curves of CoNiFe-x (x= 0, 0.2, 0.4, 0.8, 1) catalysts in Ar- and CH$_4$-saturated 0.5 M Na$_2$CO$_3$ solution with a scan rate of 20 mV s$^{-1}$, respectively. (f) the current density difference of the CoNiFe-x catalysts measured at the CH$_4$-saturated and the Ar-saturated solution.

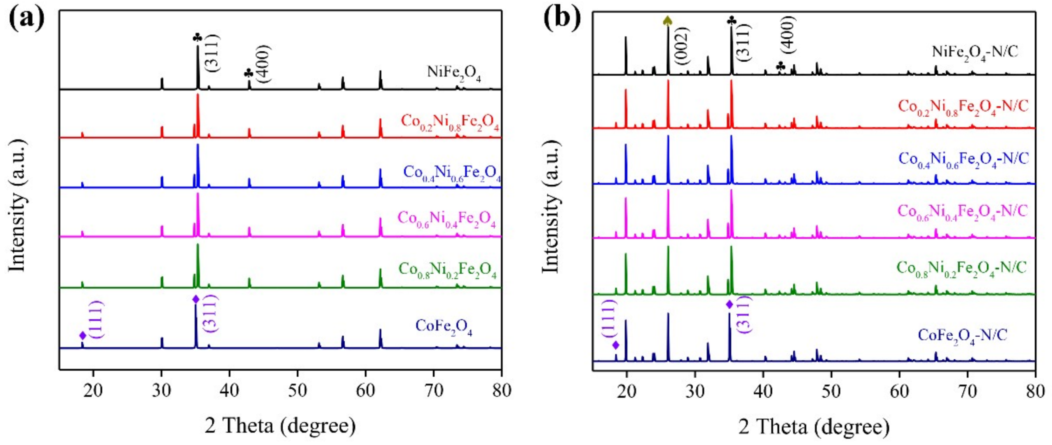

Figure S9. Simulated XRD patterns of built crystalline $Co_yNi_{1-y}Fe_2O_4$ (a) and $Co_yNi_{1-y}Fe_2O_4$-N/C (b) models.

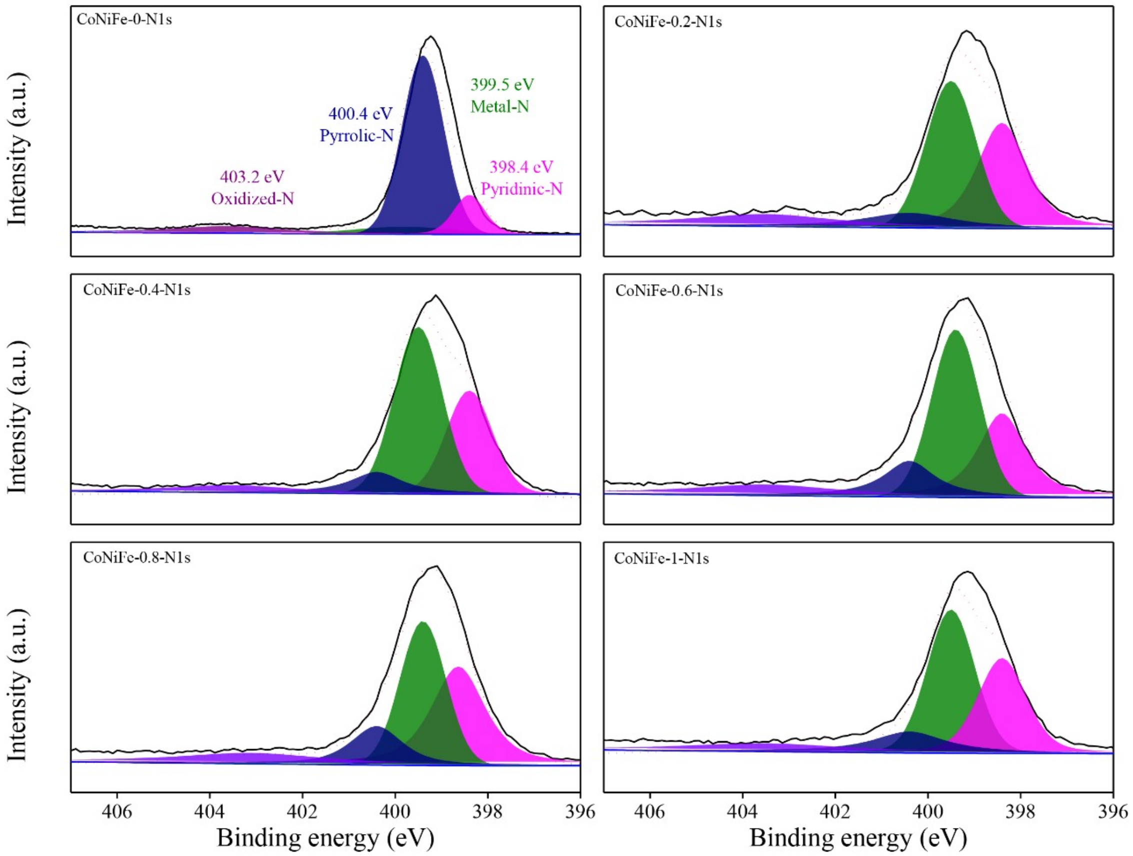

**Figure S10**. High-resolution XPS spectra of CoNiFe-N/C-x catalysts for N 1s.

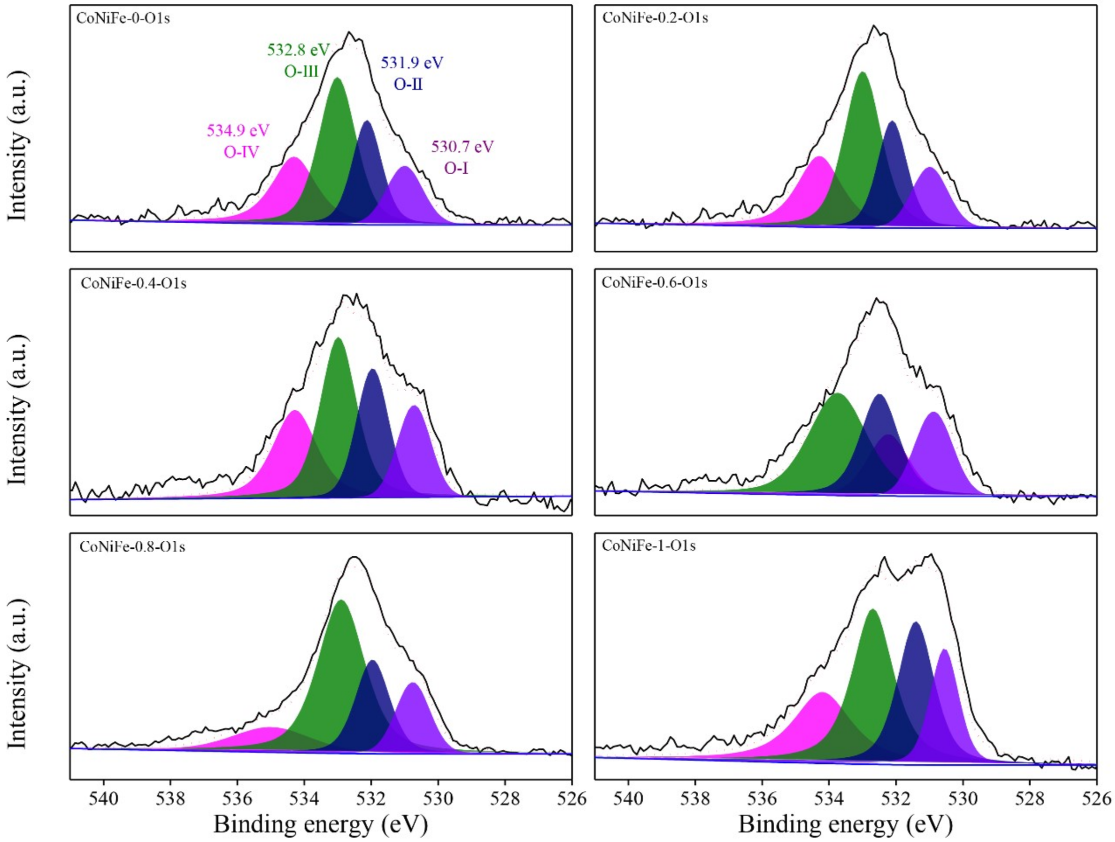

**Figure S11**. High-resolution XPS spectra of CoNiFe-N/C-x catalysts for O 1s.

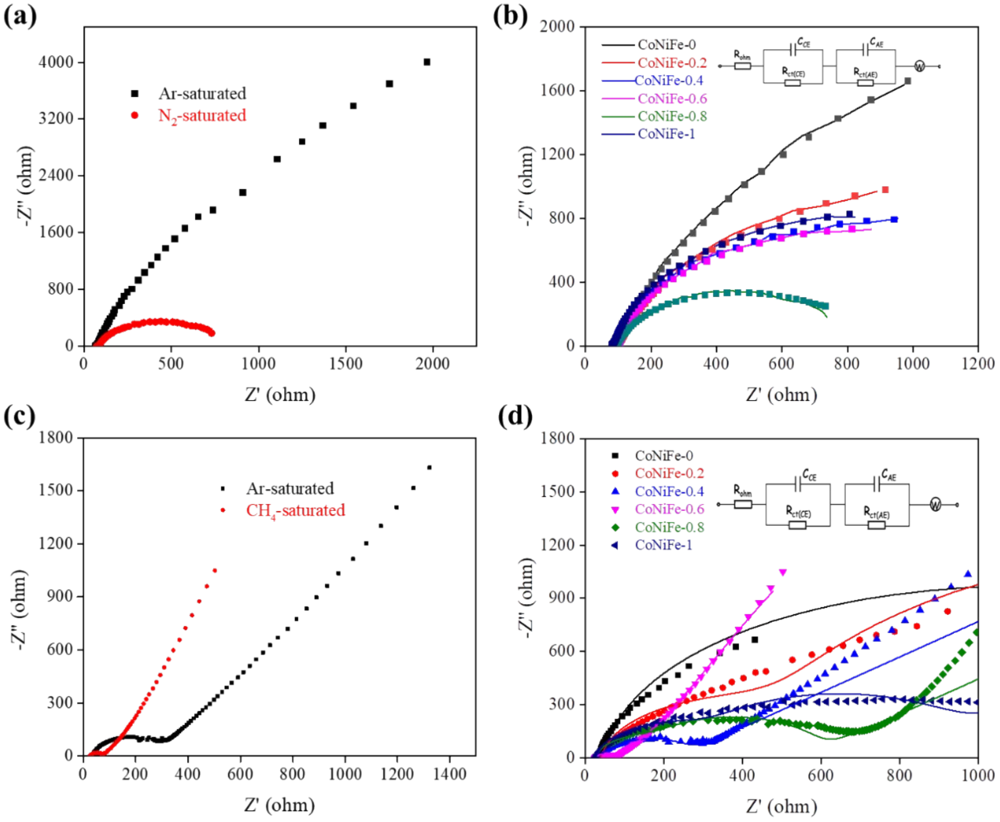

**Figure S12**. EIS spectra of: (a) $Co_{0.8}Ni_{0.2}Fe_2O_4$-N/C catalyst under the Ar- and $N_2$-saturated conditions; (b) various composition ratios of the CoNiFe-N/C catalysts under the $N_2$-saturation condition [Inset: equivalent circuit model (Point: original data; Line: fitting data)]; (c) the $Co_{0.6}Ni_{0.4}Fe_2O_4$-N/C catalyst under the Ar- and $CH_4$-saturated conditions; (d) various composition ratios of the CoNiFe-N/C catalysts under $CH_4$-saturation conditions [Inset: equivalent circuit model].

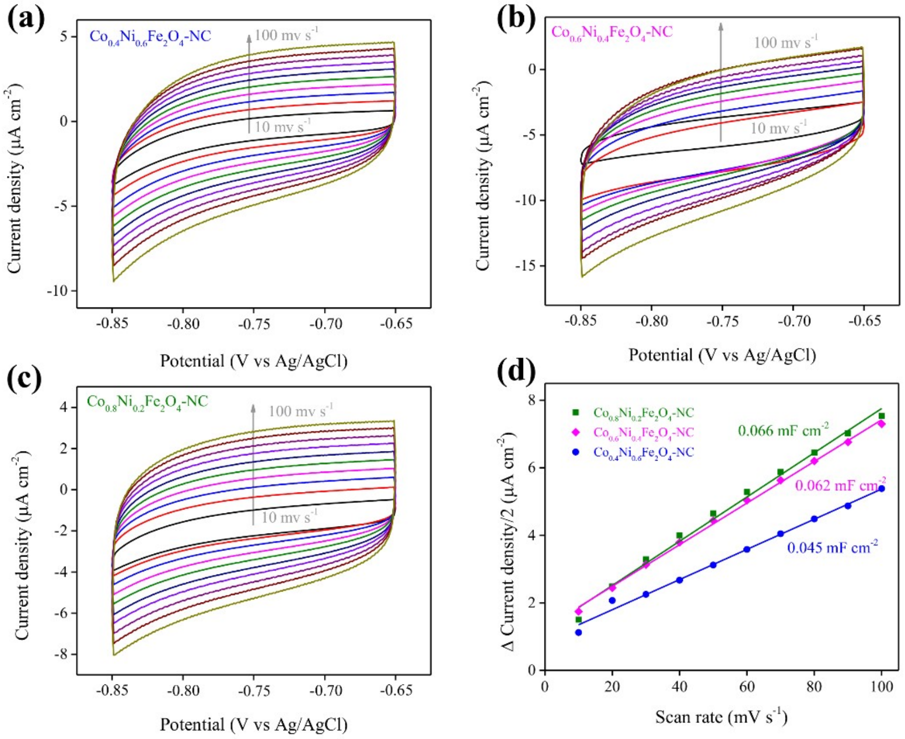

**Figure S13**. ECSA comparisons for (a) CoNiFe-N/C-0.4, (b) 0.6, (c) 0.8 composites based on their double-layer capacitances using CV at different scan rates from 10 to 100 mV $s^{-1}$ in $N_2$-saturated 0.1 M $Na_2SO_4$. (d) the corresponding plots of the current density at -0.75 V vs. the scan rate.

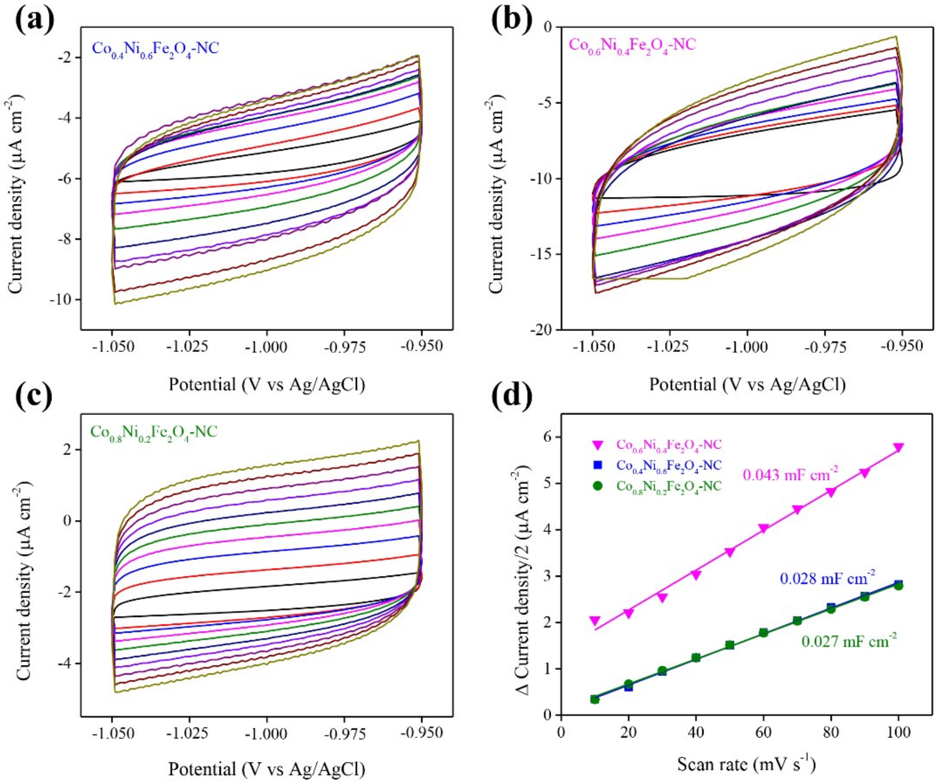

**Figure S14**. ECSA comparisons for (a) CoNiFe-N/C-0.4, (b) 0.6, (c) 0.8 composites based on their double-layer capacitances using CV at different scan rates from 10 to 100 mV s$^{-1}$ in $CH_4$-saturated 0.5 M $Na_2CO_3$. (d) the corresponding plots of the current density at 1.0 V vs. the scan rate.

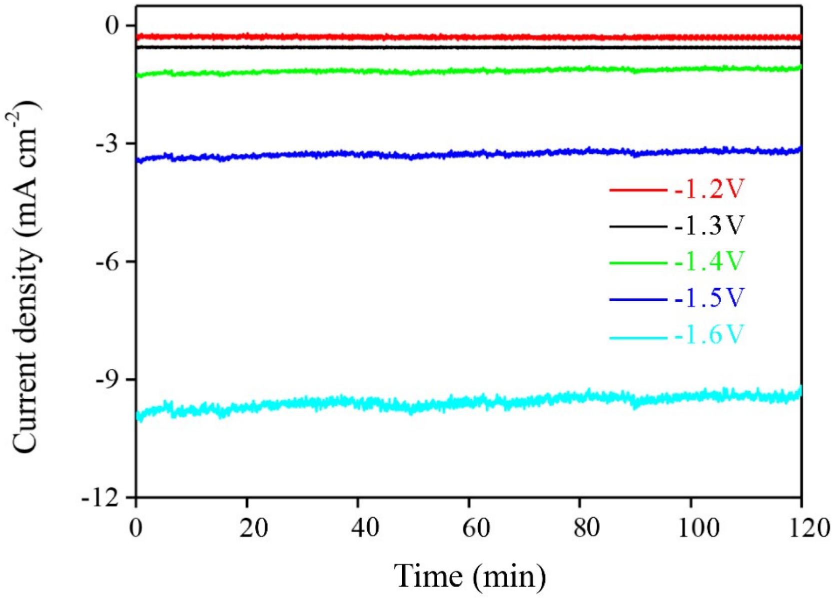

**Figure S15.** Chronoamperometric curves for the NRR recorded at different potentials over the CoNiFe-NC-0.8 catalyst.

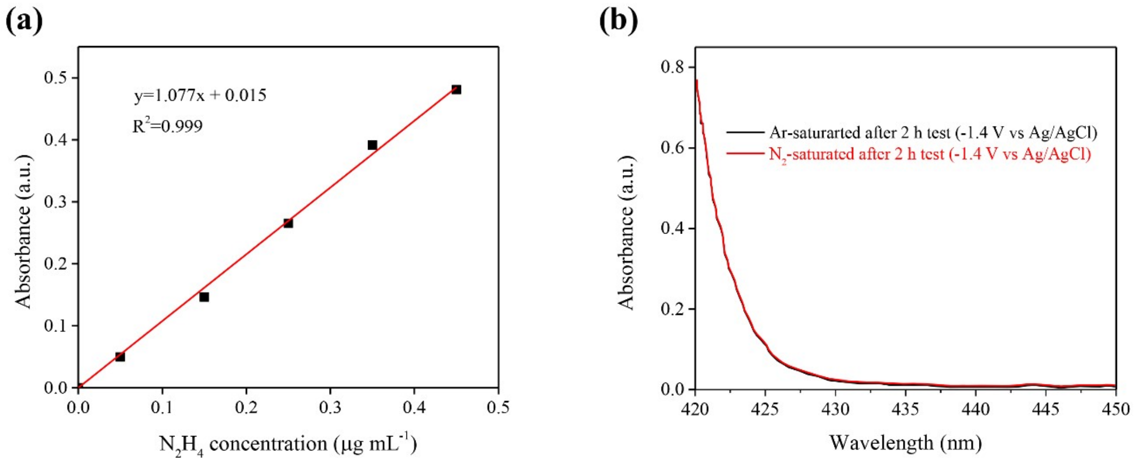

**Figure S16**. (a) Calibration curve for the detection of $N_2H_4$ concentration; (b) UV-vis spectra of the cathode chamber solution after two-hour electrolysis under an Ar- and $N_2$-saturated condition.

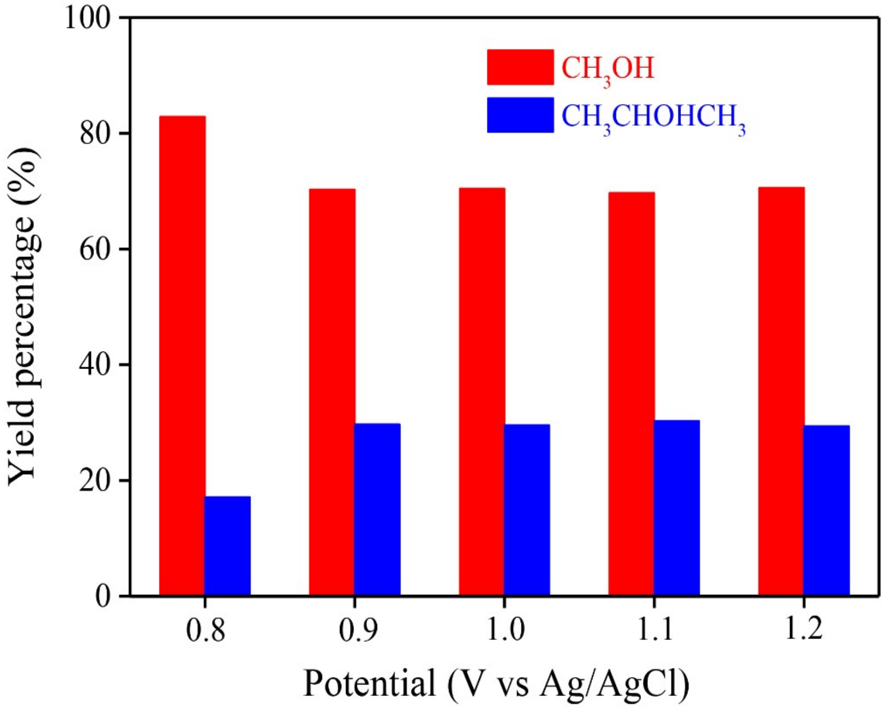

**Figure S17**. Product yield percentage of the DMC over the $Co_{0.6}Ni_{0.4}Fe_2O_4$-N/C catalyst at different applied potentials.

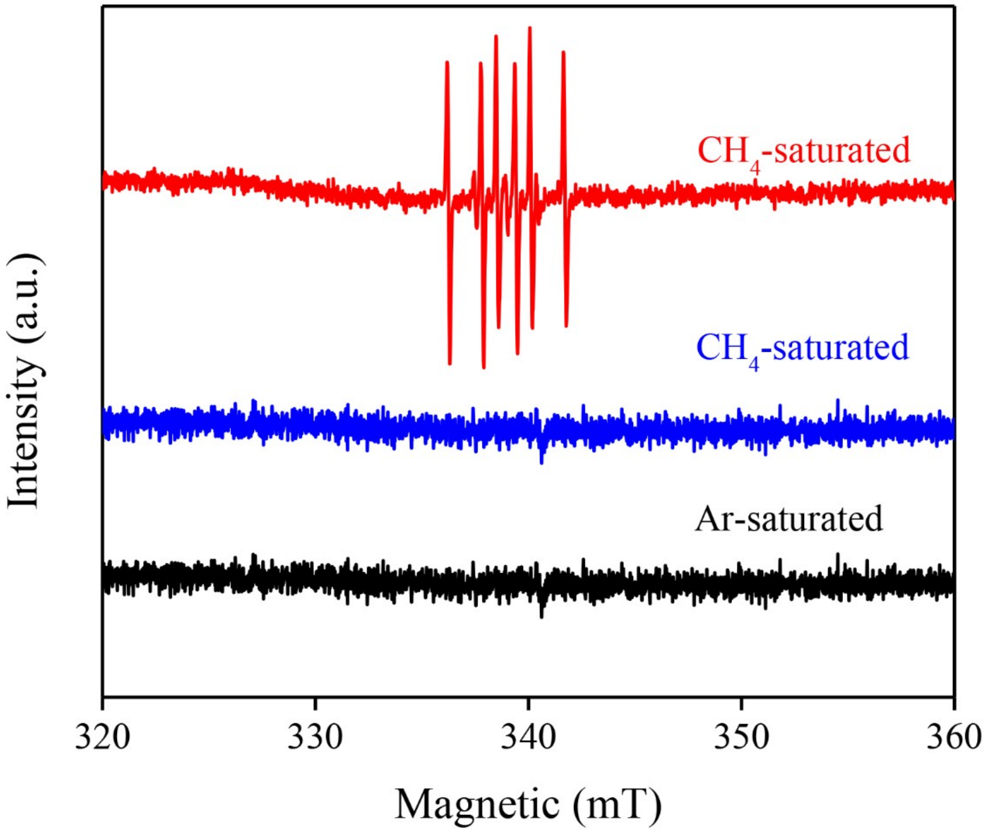

**Figure S18**. EPR spectra of the electrochemical $CH_4$ oxidation over the $Co_{0.6}Ni_{0.4}Fe_2O_4$-N/C catalyst (DMPO-$\cdot O_2^-$ formed in methanol dispersions, 0.3 M; Blue: open voltage condition; Red: with potential).

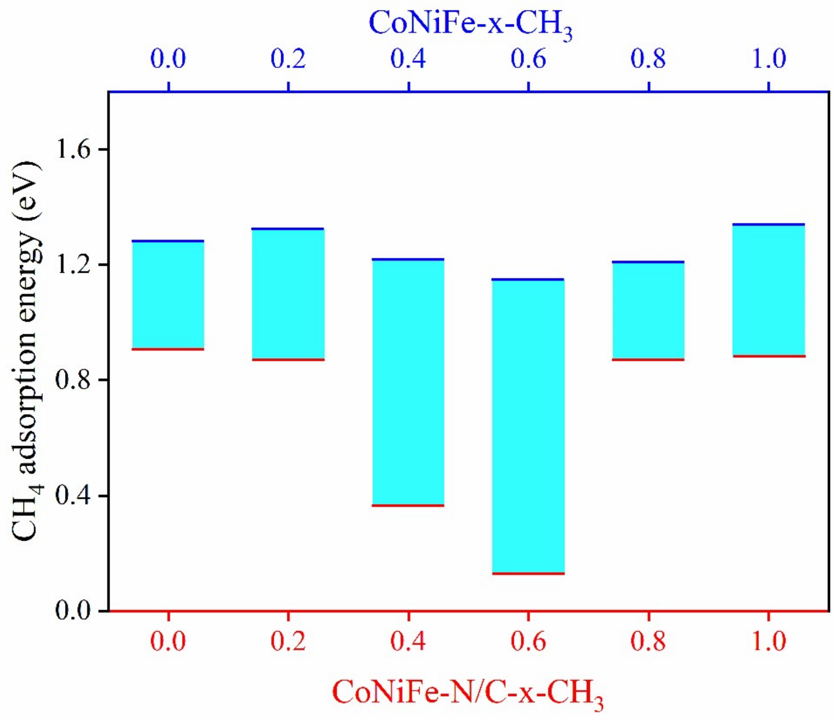

**Figure S19**. Adsorption energy comparison of the $CH_4$ absorption over the surface of CoNiFe-x and CoNiFe-N/C-x catalysts.

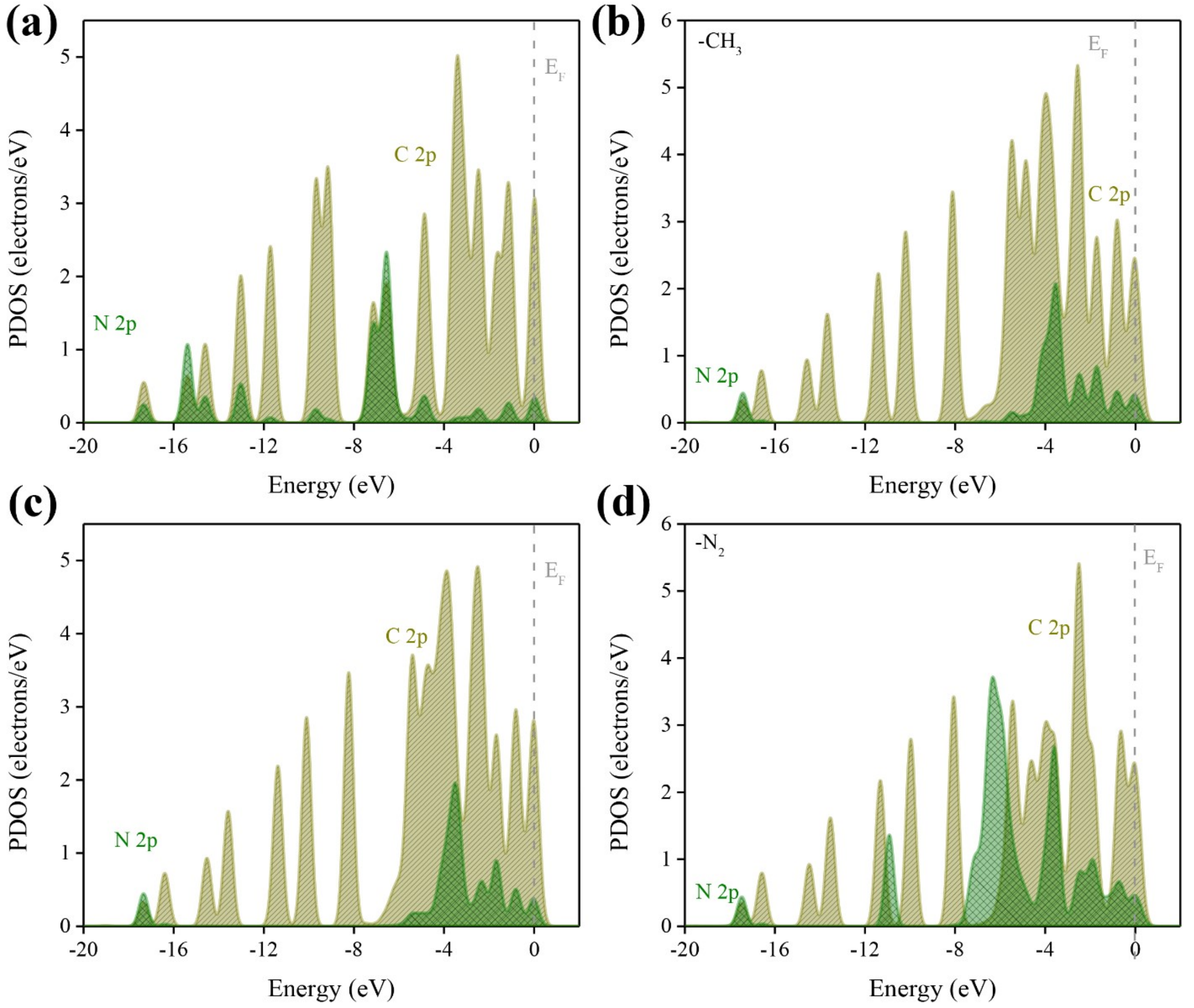

**Figure S20**. PDOS of carbon layer for (a) $Co_{0.6}Ni_{0.4}Fe_2O_4$-NC and (b) $Co_{0.6}Ni_{0.4}Fe_2O_4$-NC surface, and the corresponding $CH_4$ adsorption (c) and $N_2$ adsorption (d).

# References

1. Z. Wang, Y. Li, H. Yu, Y. Xu, H. Xue, X. Li, H. Wang and L. Wang, *ChemSusChem*, 2018, **11**, 3480-3485.
2. L. Xia, X. Wu, Y. Wang, Z. Niu, Q. Liu, T. Li, X. Shi, A. M. Asiri and X. Sun, *Small Methods*, 2018, **14**, 1800251.
3. S. Z. Andersen, V. Colic, S. Yang, J. A. Schwalbe, A. C. Nielander, J. M. McEnaney, K. Enemark-Rasmussen, J. G. Baker, A. R. Singh, B. A. Rohr, M. J. Statt, S. J. Blair, S. Mezzavilla, J. Kibsgaard, P. C. K. Vesborg, M. Cargnello, S. F. Bent, T. F. Jaramillo, I. E. L. Stephens, J. K. Norskov and I. Chorkendorff, *Nature*, 2019, **570**, 504-508.
4. L. Zeng, X. Li, S. Chen, J. Wen, W. Huang and A. Chen, *J. Mater. Chem. A*, 2020, **8**, 7339-7349.
5. X. Han, C. S. Gerke, S. Banerjee, M. Zubair, J. Jiang, N. M. Bedford, E. M. Miller and V. S. Thoi, *ACS Energy Lett.*, 2020, **5**, 3237-3243.
6. K. Chu, Y.-p. Liu, Y.-b. Li, H. Zhang and Y. Tian, *J. Mater. Chem. A*, 2019, **7**, 4389-4394.
7. M. I. Ahmed, S. Chen, W. Ren, X. Chen and C. Zhao, *Chem. Commun.*, 2019, **55**, 12184-12187.
8. J. Hou, M. Yang and J. Zhang, *Nanoscale*, 2020, **12**, 6900-6920.
9. S. Luo, X. Li, B. Zhang, Z. Luo and M. Luo, *ACS Appl. Mater. Interfaces*, 2019, **11**, 26891-26897.
10. B. Yang, W. Ding, H. Zhang and S. Zhang, *Energy Environ. Sci.*, 2021, **14**, 672-687.
11. K. Chu, Y.-p. Liu, Y.-b. Li, Y.-l. Guo and Y. Tian, *ACS Appl. Mater. Interfaces*, 2020, **12**, 7081-7090.

12. K. Lu, F. Xia, B. Li, Y. Liu, I. B. Abdul Razak, S. Gao, J. Kaelin, D. E. Brown and Y. Cheng, *ACS Nano*, 2021.
13. K. Zhao, X. Quan, Y. Su, X. Qin, S. Chen and H. Yu, *Environ. Sci. Technol.*, 2021.
14. F. Lai, J. Feng, X. Ye, W. Zong, G. He, C. Yang, W. Wang, Y.-E. Miao, B. Pan, W. Yan, T. Liu and I. P. Parkin, *J. Mater. Chem. A*, 2020, **8**, 1652-1659.
15. C. Ma, X. Yan, H. He, B. Liu and S. Yan, *Sustain. Energy Fuels*, 2021, **5**, 2415-2418.
16. J. H. Moon, M. Y. Lee, B. C. Park, Y. S. Jeon, S. Kim, T. Kim, M. J. Ko, K. H. Cho, K. T. Nam and Y. K. Kim, *Small*, 2021, e2103575.
17. C. Li, Y. Fu, Z. Wu, J. Xia and X. Wang, *Nanoscale*, 2019, **11**, 12997-13006.
18. Y. Li, J. Li, J. Huang, J. Chen, Y. Kong, B. Yang, Z. Li, L. Lei, G. Chai, Z. Wen, L. Dai and Y. Hou, Angew.Chem. Int. Ed., 2021, **60**, 9078-9085.
19. W. Ye, Y. Yang, M. Arif, S. Yang, X. Fang, M. A. Mushtaq, X. Chen and D. Yan, *ACS Sustain. Chem. Eng.*, 2020, **8**, 15946-15952.
20. Y. Wang, X. Cui, J. Zhao, G. Jia, L. Gu, Q. Zhang, L. Meng, Z. Shi, L. Zheng, C. Wang, Z. Zhang and W. Zheng, *ACS Catal.*, 2018, **9**, 336-344.
21. W. Li, D. He, G. Hu, X. Li, G. Banerjee, J. Li, S. H. Lee, Q. Dong, T. Gao, G. W. Brudvig, M. M. Waegele, D. E. Jiang and D. Wang, *ACS Cent Sci*, 2018, **4**, 631-637.
22. Y. Song, Y. Zhao, G. Nan, W. Chen, Z. Guo, S. Li, Z. Tang, W. Wei and Y. Sun, *Appl. Catal. B-Environ.*, 2020, **270**, 118888.
23. Z. Guo, W. Chen, Y. Song, X. Dong, G. Li, W. Wei and Y. Sun, *Chinese J. Catal.*, 2020, **41**, 1067-1072.
24. Y. Liu, X. Zhu, Q. Zhang, T. Tang, Y. Zhang, L. Gu, Y. Li, J. Bao, Z. Dai and J.-S. Hu, *J. Mater. Chem. A*, 2020, **8**, 8920-8926.

25. M. Ma, C. Oh, J. Kim, J. H. Moon and J. H. Park, *Appl. Catal. B-Environ.*, 2019, **259**, 118095.
26. M. Ma, B. J. Jin, P. Li, M. S. Jung, J. I. Kim, Y. Cho, S. Kim, J. H. Moon and J. H. Park, *Adv. Sci.*, 2017, **4**, 1700379.
27. C. Oh, J. Kim, Y. J. Hwang, M. Ma and J. H. Park, *Appl. Catal. B-Environ.*, 2021, **283**, 119653.
28. J. Wu, J. H. Li and Y. X. Yu, *ACS Appl. Mater. Interfaces*, 2021, **13**, 10026-10036.
29. J. Lee, J. Yang and J. H. Moon, *ACS Energy Letters*, 2021, 893-899.